Solar-Terrestrial Physics, 2018. Vol. 4. Iss. 2, pp. 63–68, DOI: 10.12737/stp-42201810. © 2018 A.A. Popov, N.M. Gavrilov, A.B. Andreev, A.I. Pogoreltsev.
Published by INFRA-M Academic Publishing House
Original Russian version: A.A. Popov, N.M. Gavrilov, A.B. Andreev, A.I. Pogoreltsev, published in Solnechno-zemnaya fizika, 2018, vol. 4, iss. 2, pp. 102–108, DOI: 10.12737/szf-42201810 © 2018 INFRA-M Academic Publishing House (Nauchno-Izdatelskii Tsentr INFRA-M

INTERANNUAL DYNAMICS IN INTENSITY OF MESOSCALE HYDROXYL NIGHTGLOW VARIATIONS OVER ALMATY

A.A. Popov
Saint-Petersburg State University,
Saint-Petersburg, Russia, Andrew.Popovix@gmail.com

N.M. Gavrilov
Saint-Petersburg State University,
Saint-Petersburg, Russia, n.gavrilov@spbu.ru

A.B. Andreev
Institute of the Ionosphere,
Almaty, Kazakhstan, alexey.andreyev@rambler.ru

A.I. Pogoreltsev
Saint-Petersburg State University,
Russian State Hydro-meteorological University,
Saint-Petersburg, Russia, apogor@rshu.ru

Abstract. The method of digital difference filters is applied to the data analysis of SATI observations of hydroxyl nightglow intensity and rotational temperature at altitudes 85–90 km over Almaty (43°03' N, 76°58' E), Kazakhstan, in 2010–2017. We examine seasonal and interannual variations in monthly average values and standard deviations of variations with periods 0.4–5.4 hrs, which may be associated with internal gravity waves in the mesopause region. The monthly average temperature near the mesopause has a maximum in winter and a minimum in June. The monthly average intensity has an additional maximum in June. Standard deviation of mesoscale rotational temperature variations and characteristics of internal gravity waves are maximum in spring and autumn. The spring maximum of mesoscale OH emission intensity variations is shifted to June. Interannual variations and multi-year trends of OH rotational temperature and emission intensity may differ in detail. This may be connected with seasonal and long-term variations in the complex system of the photochemical processes, which produce the OH nightglow.

Keywords: upper atmosphere, nightglows, hydroxyl, intensity, rotational temperature, climatology, seasonal variations, trends, mesoscale variability, internal gravity waves.

INTRODUCTION

Considerable attention is being given to internal gravity waves (IGW) in the middle and upper atmosphere. Their sources are generally located in the lower atmosphere. Propagating upward, IGW can transfer energy and momentum to the middle and upper atmosphere, thus influencing thermodynamic processes throughout the atmosphere. Measuring nightglow intensity and rotational temperature is one of the methods of monitoring the thermodynamic regime and composition of the upper atmosphere.

Propagating through the nightglow layer, IGW modulate its temperature and intensity [Shefov et al., 2006]. Coherent wave-like structures have been found in OH, Na, O, and O_2 emission layers in an altitude range 80–100 km [Krassovski, 1972; Krasovski et al., 1978; Gavrilov, Shved, 1982; Taylor et al., 1987]. Swenson and Mende [1994] observed quasi-monochromatic IGW and wave breaking processes, with subsequent formation of vortex structures in the OH nightglow. Taylor, Hapgood [1990] and Vadas et al. [2009] have found wave structures with horizontal wavelengths 5–l60 km in the OH airglow. Observations in Shigaraki, Japan, have revealed typical IGW parameters in the OH airglow: 5–60 km horizontal wavelengths, 5–30 min periods, 0–100 m/s horizontal phase velocities [Nakamura et al., 1999].

A number of studies have dealt with long-term variations in IGW intensity in the upper atmosphere. Gavrilov et al. [2002b] have carried out a statistical analysis of medium and large-scale IGW with 0.5–5 hr periods and 100–1700 km wavelengths in the OH and O_2 emissions in a period from 1998 to 2001. Interannual and seasonal mesopause temperature variations have been also studied using spectral observations of hydroxyl emission made in Zvenigorod and Irkutsk in a period 2000–2010 [Perminov et al., 2014]. Medvedeva et al. [2011] and Pertsev et al. [2013] have investigated the variability of characteristics of the mesopause region during sudden stratospheric warming events. Recent studies have revealed the presence of long-term variations in characteristics of the upper atmosphere [Laštovička, 2017].

Gavrilyeva et al. [2009] have analyzed variations in the OH nightglow intensity and rotational temperature under the effect of atmospheric tides. Somsikov et al. [2015] examined mean characteristics of IGW in the OH emission layer over Almaty in a period 2010–2015. They determined that the major contribution to mesoscale variations of the OH emission layer is made by IGW with horizontal wavelengths 100–900 km. Similar values of IGW horizontal wavelengths have been obtained in the analysis of Spectral Airglow Temperature Imager (SATI) observations of OH and O_2 emissions in Shigaraki, Japan [Gavrilov et al., 2002b]. The study of O_2 nightglow variations with MORTI in Almaty

has given even greater IGW horizontal wavelengths – up to several thousand kilometers [Aushev et al., 2000].

Gavrilov et al. [2001] using simple difference filters have analyzed seasonal and interannual variations in IGW intensity at 80–100 km from observations of drifts of meteor trails and ionospheric irregularities. This method proved to be effective for the analysis of long-term variations in IGW intensity in the upper atmosphere [Gavrilov et al., 1995, 2002a].

In this paper, we adopt the method of digital difference filters to analyze SATI observations of hydroxyl nightglow and rotational temperature at 85–90 km over Almaty, Kazakhstan, in 2010–2017. We examine seasonal and interannual variations in the average temperature and intensity, which may be associated with IGW propagation in the mesopause region, in three period bands covering a range 0.4–5.4 hrs.

1. INSTRUMENT AND DATA ANALYSIS METHOD

Data on hydroxyl nightglow at altitudes 85–90 km in a period 2010–2017 have been obtained at the Institute of the Ionosphere in Almaty, Kazakhstan. We used the Spectral Airglow Temperature Imager (SATI) installed in the Tien Shan foreland. Measurements were made at a high mountain complex of the Institute of the Ionosphere (43°03′ N, 76°58′ E) at an altitude of 2730 m above sea level. The instrument in use is a Fabry—Perot spectrometer in which the etalon is a narrowband interference filter and the detector is a CCD camera. SATI measures the rotational temperature and nightglow intensity in the hydroxyl (6-2) band. To identify the band, SATI uses an interference filter with a bandwidth centered at 836.813 nm [Lopez-Gonzalez et al., 2007]. The temperature is determined by comparing the measured spectrum of OH (6-2) bands with model spectra calculated for different hydroxyl vibration-rotation temperatures. The exposure time is 1 min. The use of SATI to study IGW-induced mesoscale variations in the lower thermosphere is described in detail by Wiens et al. [1997].

SATI measures the OH emission intensity and rotational temperature at a mean altitude of 87 km at twelve points of the sky along the night sky ring with a diameter of about 100 km and a width of 14 to 16 km (see Figure 1 in [Somsikov et al., 2015]). In the primary processing, the measured values are averaged over the twelve points of the sky and over Δt intervals. The comparison between the OH rotational temperature, measured with SATI over Almaty, and satellite data [Pertsev et al., 2013] has shown that the discrepancies do not exceed several Kelvin.

To evaluate the intensity of mesoscale disturbances in the mesopause region, we adopt the method described by Gavrilov et al. [2001]. We use numerical filtering by computing differences between successive Δt-averages of the estimated nightglow characteristic f:

$$f_i' = \left(f_{i+1} - f_i \right) / 2, \qquad (1)$$

where i is the number of the Δt interval with the midpoint t_i. Gavrilov et al. [2001] have shown that this difference between Δt averages is equivalent to the numerical frequency filter with a transmission function

$$H^2 = \frac{\sin^4(\sigma \Delta t / 2)}{(\sigma \Delta t / 2)^4}, \qquad (2)$$

where σ is the frequency, $\Delta t = t_{i+1} - t_i$ is the time step of successive intervals. Figure 1 presents transmission functions of filter (2) for different values of Δt.

In the frequency domain, bandwidths of the filters with Δt=0.25 hr and Δt=0.5 hr are respectively four and two times wider than the bandwidth of a lower-frequency filter with Δt=1 hr. Data averaging over the annular domain of the airglow layer of ~100 km in diameter, observed with SATI (see above), excludes from consideration the disturbances with horizontal scales of less than 100 km.

To improve the statistical reliability, filtering (1) is carried out only for pairs of adjacent intervals, containing at least 67 % of minute data records in each of the intervals. To analyze seasonal and interannual variations, we calculate monthly averages and relative standard deviations of differences (1) for each calendar month of hydroxyl nightglow observations.

Maxima of H^2 and boundaries of the half-width of the transmission functions, shown in Figure 1, at a level of 0.5 from maxima are listed in Table.

Table

Periods τ_m corresponding to H^2 maxima and low-frequency τ_0 and high-frequency τ_h boundaries of the bandwidth at 0.5 from maxima of the transmission functions shown in Figure 1

Δt, hr	τ_m, hr	τ_0, hr	τ_h, hr
1	2.8	5.4	1.7
0.5	1.4	2.7	0.8
0.25	0.7	1.3	0.4

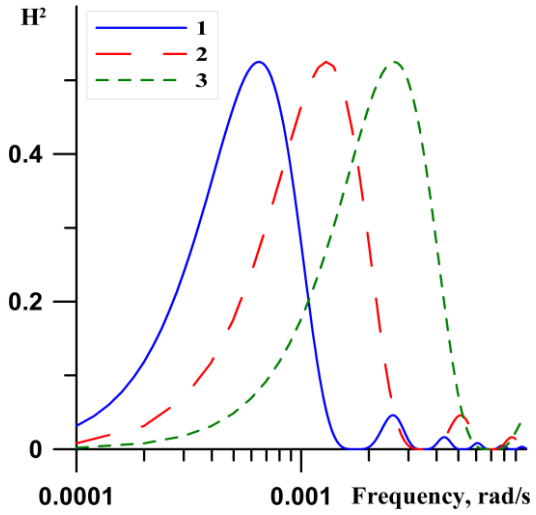

Figure 1. Transmission functions of difference filter (2) for Δt: 1 hr – 1; 0.5 hr – 2; 0.25 hr – 3

2. OH ROTATIONAL TEMPERATURE VARIABILITY

We adopt the method described in Section 1 to process SATI ground-based observations of OH (6-2) band nightglow intensity and rotational temperature over Almaty from May 2010 to April 2017. One of the causes of mesoscale nightglow variations may be IGW propagating in the airglow layer. Polarization relations of the theory of atmospheric IGW [Gossard, Hooke, 1978] yield the following formulas relating the amplitude of wave variations of horizontal velocity U and potential wave energy E_p to average temperature and its mesoscale variance:

$$U = \frac{g}{N}\sqrt{\frac{\overline{T'^2}}{T_0^2}}, E_p = \frac{U^2}{2}, \quad (3)$$

where g is the acceleration due to gravity, N is the Brunt—Väisälä frequency, T_0 is the average temperature, $\overline{T'^2}$ is the variance of data differences (1).

Figure 2 depicts seasonal variations in monthly averages and relative standard deviations of the OH rotational temperature and IGW parameters (3) averaged over 2010–2017. Monthly average temperatures near the mesopause (Figure 2, *a*) have a maximum in winter and a minimum in summer, in June.

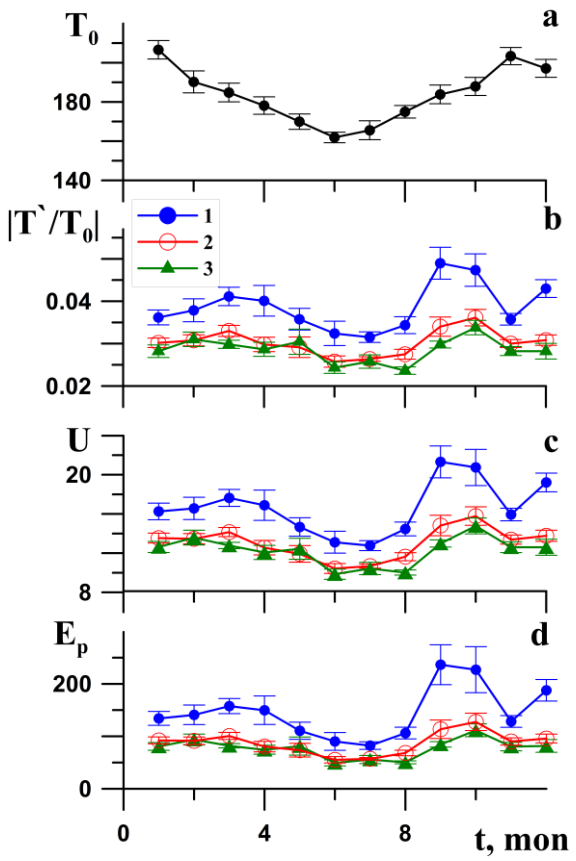

Figure 2. Seasonal variations in: monthly average temperature, K (*a*); relative standard deviation of mesoscale temperature variations (*b*); amplitudes of horizontal velocity disturbances, m/s (*c*); potential wave energy, J/kg, (*d*) averaged over 2010–2017 using differential filter (1) with Δt: 1 hr — 1; 0.5 hr — 2; 0.25 hr — 3

Intensities of mesoscale temperature variations (Figure 2, *b*) and IGW characteristics in all frequency ranges (Figure 2, *c* , *d*) are maximum in spring and autumn and minimum in winter and summer for all frequency bands. A similar seasonal variation of IGW intensities with the main autumn maximum and smaller spring maximum was obtained by Gavrilov and Shved [1982] while analyzing wave variations in the OI 557.7 nm nightglow in Ashkhabad. Spring and autumn maxima of IGW intensities were also identified from radar wind observations at altitudes 80–100 km by Gavrilov et al. [2003] and from SATI observations in Shigaraki [Gavrilov et al., 2002b].

Figure 3 shows interannual variations in the OH rotational temperature in a period from 2010 to 2017. Thin lines are polynomial quadratic approximations. The average temperature near the mesopause in Figure 3, *a* exhibits periodic changes in accordance with the seasonal variation shown in Figure 2, *a*. The regression line is qualitatively consistent with negative temperature trends at 80–100 km altitudes, determined from satellite and ground-based measurements [Laštovička, 2017].

Mid-latitude observations have shown that the negative temperature trend, which is determined after excluding the influence of solar activity, is of order of –(0.2÷0.3) K per year at these altitudes [Perminov et al., 2014].

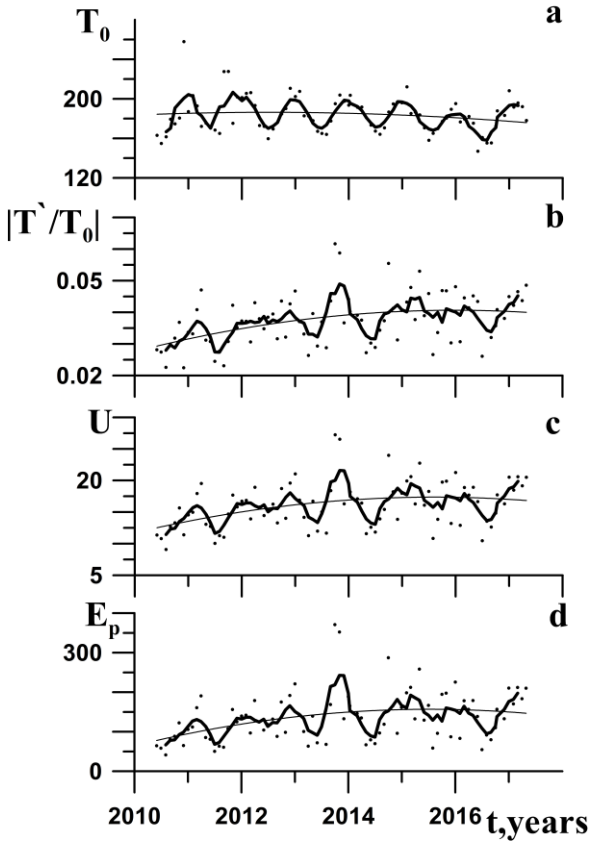

Figure 3. Interannual variations in: monthly average temperature, K (*a*); relative standard deviation of mesoscale temperature variations (*b*); amplitudes of horizontal velocity disturbances, m/s (*c*); potential wave energy, J/kg, (*d*) within a range of periods τ~1.7–5.4 hrs. Thick lines indicate 4-month moving averages; thin lines are quadratic approximations by a least squares method

Interannual temperature variations shown in Figure 5, *a* have more significant trends. They may be caused by interannual variations in solar activity, which has a positive correlation with the OH rotational temperature [Perminov et al., 2014; Ammosov et al., 2014]. We cannot, however, exclude the influence of time variations in measuring instrument characteristics, either.

Relative variations in OH emission intensity and rotational temperature may be more resistant to slow changes in these characteristics. Figure 3 *b–d* shows interannual variations in characteristics of mesoscale variations with 1.7–5.4 hr periods. These variations are less periodic than the average temperature variations in Figure 3, *a*. This is due to the more complicated seasonal variations in the same characteristics in Figure 2, *b–d* and their greater instability in different years. The polynomial quadratic approximations in Figure 3, *b–d* show long-term variations in the intensity of mesoscale disturbances near the mesopause. Similar IGW intensity variations were obtained from observations of mesoscale wind speed variations in the upper atmosphere [Gavrilov et al., 2001, 2002a].

The values $|T'/T_0|$ and E_p in Figures 2, 3 exceed the estimated IGW values derived from OH emission observations in Zvenigorod and Tory [Perminov et al., 2014]. Perhaps this is due to the use of another method of frequency and spatial data filtering, which may result in differences between portions of the IGW spectrum under study. Besides, we do not apply correction for random noise generated by instrument measurement errors.

3. Variability of OH emission intensity

Figure 4, *b* depicts the seasonal variation in the OH nightglow intensity I averaged over 2010–2017. By comparison, Figure 4, *a* show again the seasonal variation of OH rotational temperature presented in Figure 2, *a*. It is seen that, unlike T_0, the average OH emission intensity I_0, except for the winter maximum, has an additional summer maximum (Figure 4, *b*). Similar differences between the I_0 and T_0 seasonal variations have been obtained for Almaty and Zvenigorod in [Shefov et al., 1969]. Differences between seasonal variations in I_0 and T_0 may be associated with circulation variations, which can affect gas composition, rate of photochemical reactions, ratio of OH mixture, and height of the airglow layer.

Figure 4, *e* shows seasonal variations in the relative mesoscale dispersion of OH emission intensity $|I'/I_0|$. The comparison of this plot with the plot of $|T'/T_0|$ (Figure 4, *c*) reveals a shift of the spring maximum of $|I'/I_0|$ to June and its larger value. Mesoscale nightglow variations are often analyzed using the ratio

$$\eta = \left|I' / I_0\right| / \left|T' / T_0\right|. \quad (4)$$

Seasonal η variations are shown in Figure 4, *e*; η reaches the main maximum in June synchronously with the summer maximum of I_0 (Figure 4, *b*). Gavrilov and Yudin [1982] have derived an analytical expression for η, using a simple photochemical model of OH airglow

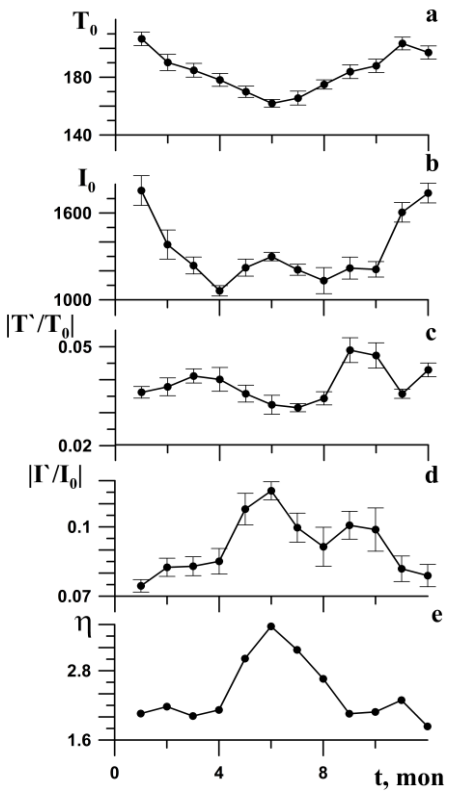

Figure 4. Seasonal variations averaged over 2010–2017 in: rotational temperature, K (*a*); OH emission intensity, arbitrary relative units (*b*); relative mesoscale standard deviations of temperature and intensity, respectively (*c*, *d*); η for τ~1.7–5.4 hr (*e*)

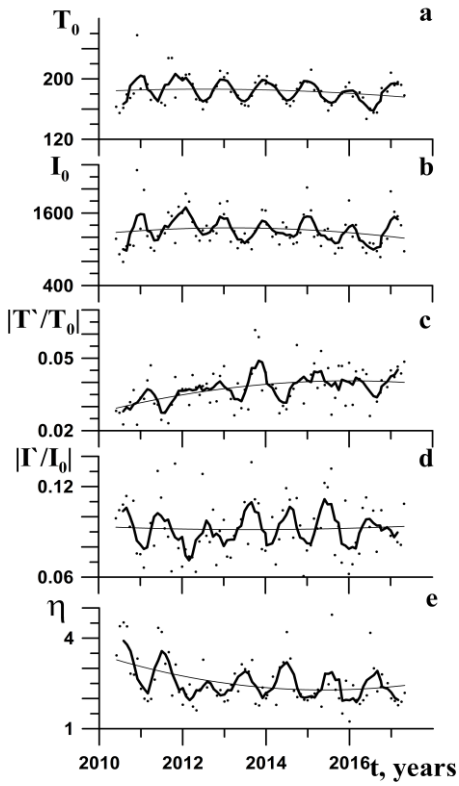

Figure 5. Interannual variations in: monthly average rotational temperature, K (*a*); OH emission intensity, arbitrary relative units (*b*); relative mesoscale standard deviations of temperature and intensity respectively (*c* , *d*); η for τ~1.7–5.4 hrs (*d*).

Thick lines show 5-month moving averages; thin lines are quadratic approximations by the least squares method

and the linear theory of atmospheric IGW. The theoretically estimated η~1.9–2.5 corresponds to most values in Figure 4 *e*.

Interannual variations in T_0, I_0, $|T'/T_0|$, $|I'/I_0|$, and η are shown in Figure 5. Thin lines indicate polynomial quadratic approximations by the least squares method. It is seen that interannual variations in OH rotational temperature and airglow intensity may differ in detail. This may be associated with seasonal and long-term variations in the complex system of photochemical processes generating the OH nightglow. For example, to estimate seasonal and interannual variations in η according to the approach of Gavrilov and Yudin [1982] requires knowing vertical profiles of O, O_3, H, HO_2, and OH at 70–110 km and their variations over several years.

Furthermore, the observed long-term variations can be sensitive to measurement errors, which may differ for different instruments. To evaluate the influence of these differences, we should compare the results obtained by the proposed IGW filtering method from OH emission observations with different instruments.

CONCLUSION

Method of digital difference filters (1) and (2) has been used to analyze SATI observations of the OH rotational temperature and nightglow intensity at altitudes 85–90 km over Almaty, Kazakhstan (43°03′ N, 76°58′ E) in a period 2010–2017. We have examined seasonal and interannual changes in average temperature and intensity variations with periods from 0.4 to 5.4 hrs, which may be associated with IGW propagation in the mesopause region. To isolate mesoscale variations, we have carried out numerical filtering by computing differences between successive Δ*t*-average OH nightglow characteristics. Monthly average temperatures near the mesopause (Figure 2, *a*) have a maximum in winter and a minimum in summer, in June. Unlike the average temperatures, monthly average intensities, except for the winter maximum, have an additional maximum in June. Standard deviations of mesoscale variations in OH rotational temperature and IGW characteristics (Figure 2, *b–d*) are maximum in spring and autumn, and minimum in winter and summer. The spring maximum for mesoscale OH nightglow intensity variations (Figure 4, *d*) is shifted to June. Interannual variations in OH rotational temperature and nightglow intensity may differ in detail. This is attributed to seasonal and long-term variations in the complex system of photochemical processes producing the OH nightglow.

We are grateful to G.M. Shved for useful suggestions. This work was supported by the Russian Foundation for Basic Research (grant No. 17-05-0458).

REFERENCES

Ammosov P., Gavrilyeva G., Ammosova A., Koltovskoi I. Response of the mesopause temperatures to solar activity over Yakutia in 1999-2013. *Adv. Space Res*. 2014, vol. 54, pp. 2518–2524. DOI: 10.1016/j.asr.2014.06.007.

Aushev V.M., Pogoreltsev A.I., Vodyannikov V.V., Wiens R.H., Shepherd G.G. Results of the airglow and temperature observations by MORTI at the Almaty site (43.05 N, 76.97 E). *Physics and Chemistry of the Earth. (Part B)*. 2000, vol. 25, no. 5–6, pp. 409–415. DOI: 10.1016/S1464-1909(00) 00035-6.

Gavrilov N.M., Shved G.M. A study of internal gravity waves in the lower thermosphere based on skyglow isophots. *Izvestiya AN SSSR. Fizika atmosfery i okeana* [Izvestiya, Atmospheric and Oceanic Physics]. 1982, vol. 18, no. 1, pp. 5–12.

Gavrilov N.M., Manson A.H., Meek C.E. Climatological monthly characteristics of middle atmosphere gravity waves (10 min – 10 hr) during 1979–1993 at Saskatoon. *Ann. Geophys*. 1995, vol. 13, no. 1, pp. 285–295. DOI: 10.1007/s00585-995-0285-7.

Gavrilov N.M., Jacobi Ch., Kurschner D. Climatology of ionospheric drift perturbations at Collm, Germany. *Adv. Space Res*. 2001, vol. 27, no. 10, pp. 1779–1784. DOI: 10.1016/S0273-1177(01)00339-8.

Gavrilov N.M., Fukao S., Nakamura T., Jacobi C., Kürschner D., Manson A. H., Meek C.E. Comparative study of interannual changes of the mean winds and gravity wave activity in the middle atmosphere over Japan, Central Europe and Canada. *J. Atmos. Solar-Terr. Phys*. 2002a, vol. 64, no. 8–11, pp. 1003–1010. DOI: 10.1016/S1364-6826(02)00055-X.

Gavrilov N.M., Shiokawa K., Ogawa T. Seasonal variations of medium-scale gravity wave parameters in the lower thermosphere obtained from SATI observations at Shigaraki, Japan. *J. Geophys. Res*. 2002b, vol. 107, no. D24, 4755. DOI: 10.1029/2001JD001469.

Gavrilov N.M., Riggin D.M., Fritts D.C. Medium-frequency radar studies of gravity-wave seasonal variations over Hawaii (22° N, 160° W). *J. Geophys. Res*. 2003, vol. 108, no. D20, 4655. DOI: 10.1029/2002JD003131.

Gavrilyeva G.A., Ammosov P.P., Koltovskoi I.I. Semidiurnal thermal tide in the mesopause region over Yakutia. Geomagnetism and Aeronomy. 2009, vol. 49, no. 1, pp. 110–114. DOI: 10.1134/S0016793209010150.

Gossard E.E., Hooke W.H. *Volny v atmosphere* [Waves in the atmosphere]. Moscow, Mir Publ., 1978, 532 p. (In Russian). English edition: Gossard E.E., Hooke W.H. Waves in the atmosphere. New York, Elsevier Scientific Publishing Company, 1975, 456 p.

Krassovski V.I. Infrasonic variations of OH emission in the upper atmosphere. *Annales de Géophysique*. 1972, vol. 28, pp. 739–746.

Krasovsky V.I., Potapov B.P., Semenov A.I., Sobolev V.G., Shagayev M.M., Shefov N.N. Internal gravity waves near the mesopause. 1. Results of investigation of the hydroxyl emission. *Polyarnye siyaniya i svechenie nochnogo neba* [Aurora and Nigthglow]. Moscow, Sovetskoe Radio Publ., 1978, no. 26, pp. 5–29. (In Russian).

Laštovička J. A review of recent progress in trends in the upper atmosphere. *J. Atmos. Solar-Terr. Phys*. 2017, vol. 163, pp. 2–13. DOI: 10.1016/j.jastp.2017.03.009.

Lopez-Gonzalez M.J., Rodriguez E., Wiens R.H., Shepherd G.G., Sargoytchev S., Brown S., Shepherd M.G., Aushev V.M., López-Moreno J.J., Rodrigo R., Cho Y.-M. Seasonal variations of O_2 atmospheric and OH (6-2) airglow and temperature at midlatitudes from SATI observations. *J. Atmos. Solar-Terr. Phys*. 2007, vol. 69, no. 17–18, pp. 2379–2390. DOI: 10.1016/j.jastp.2007.07.004.

Medvedeva I.V., Beletsky A.B., Perminov V.I. Semenov A.I., Shefov N.N. Atmosphere temperature variations in the mesopause and lower thermosphere during stratospheric warmings from data of ground-based and satellite measurements in different longitudinal sectors. *Sovremennye problemy distantsionnogo zondirovaniya Zemli iz kosmosa* [Current Problems in Remote Sens-

ing of the Earth from Space]. 2011, vol. 8, no. 4, pp. 127–135. (In Russian).

Nakamura T., Higashikawa A., Tsuda T., Matsushita Y. Seasonal variations of gravity wave structures in OH airglow with a CCD imager at Shigaraki. *Earth, Planets, Space*. 1999, vol. 51, pp. 897–906. DOI: 10.1186/BF03353248.

Perminov V.I., Semenov A.I., Medvedeva I.V. Pertsev N.N. Temperature variations in the mesopause region according to the hydroxyl-emission observations at midlatitudes. Geomagnetism and Aeronomy. 2014, vol. 54, no. 2, pp 230–239. DOI: 10.1134/S0016793214020157.

Pertsev N.N., Andreyev A.B., Merzlyakov E.G., Perminov V.I. Mesosphere-thermosphere manifestations of stratospheric warmings: joint use of satellite and ground-based measurements. *Sovremennye problemy distantsionnogo zondirovaniya Zemli iz kosmosa* [Current Problems in Remote Sensing of the Earth from Space]. 2013, vol. 10, no. 1, pp. 93–100. (In Russian).

Shefov N.N. Hydroxyl emission of the upper atmosphere - I. *Planet. Space Sci*. 1969, vol. 17, pp. 797–813. DOI: 10.1016/0032-0633(69)90089-0.

Shefov N.N., Semenov A.I., Khomich V.Yu. Emission of the upper atmosphere as an indicator of its structure and dynamics. Moscow, GEOS Publ., 2006, 741 p. (In Russian).

Somsikov V.M., Andreyev A.B., Zhumabayev B.T. Peculiarities of seasonal behavior of wave disturbances in the mesosphere according to SATI and satellite observations. *Izvestiya Natsional'noi akademii nauk Respubliki Kazakhstan* [News of NAS RK. Physico-Mathematical Series]. 2015, vol. 4, no. 302, pp. 33–39. (In Russian).

Swenson G.R., Mende S.B. OH emission and gravity waves (including a breaking wave) in all-sky imagery from Bear Lake, UT. *Geophys. Res. Lett*. 1994, vol. 21, no. 20, pp. 2239–2242.

Taylor M.J., Hapgood M.A. On the origin of ripple-type wave structure in the OH nightglow emission. *Planet. Space Sci*. 1990, vol. 38, no. 11, pp. 1421–1430. DOI: 10.1016/0032-0633(90)90117-9.

Taylor M.J., Hapgood M.A., Rothwell P. Observations of gravity wave propagation in the OI (557.7 nm), Na (589.2 nm) and the near infrared OH nightglow emissions. *Planet. Space Sci*. 1987, vol. 35, no. 4, pp. 413–427. DOI: 10.1016/0032-0633(87)90098-5.

Vadas S.L., Taylor M.J., Pautet P.-D., Stamus P.A., Fritts D.C., Liu H.-L., Šao Sabbas F.T., Rampinelli V.T., Batista P., Takahashi H. Convection: the likely source of the medium-scale gravity waves observed in the OH airglow layer near Brasilia, Brazil, during the SpreadFEx campaign. *Ann. Geophys*. 2009, vol. 27, pp. 231–259. DOI: 10.5194/angeo-27-231-2009.

Wiens R.H., Moise A., Brown S., Sargoytchev S., Peterson R.N., Shepherd G.G., Lopez-Gonzalez M.J. Lopez-Moreno J.J., Rodrigo R. SATI: A spectral airglow temperature imager. *Adv. Space Res*. 1997, vol. 19, pp. 677–680. DOI: 10.1016/S0273-1177(97)00162-2.

How to cite this article

Popov A.A., Gavrilov N.M., Andreev A.B., Pogoreltsev A.I. Interannual dynamics in intensity of mesoscale hydroxyl nightglow variations over Almaty. *Solar-Terrestrial Physics*. 2018. vol. 4, iss. 2. pp. 63–68. DOI: 10.12737/stp-42201810.